

# Entanglement entropy scaling in critical phases of 1D quasiperiodic systems

Miguel Gonçalves<sup>1,2</sup>

<sup>1</sup>*CeFEMA-LaPMET, Departamento de Física, Instituto Superior Técnico, Universidade de Lisboa, Av. Rovisco Pais, 1049-001 Lisboa, Portugal*

<sup>2</sup>*Centro de Física das Universidades do Minho e Porto, Departamento de Física e Astronomia, Faculdade de Ciências, Universidade do Porto, 4169-007 Porto, Portugal*

We study the scaling of the entanglement entropy in different classes of one-dimensional fermionic quasiperiodic systems with and without pairing, focusing on multifractal critical points/phases. We find that the entanglement entropy scales logarithmically with the subsystem size  $N_A$  with a proportionality coefficient  $\mathcal{C}$ , as in homogeneous critical points, apart from possible additional small oscillations. In the absence of pairing, we find that the entanglement entropy coefficient  $\mathcal{C}$  is non-universal and depends significantly and non-trivially both on the model parameters and electron filling, in multifractal critical points. In some of these points,  $\mathcal{C}$  can take values close to the homogeneous (or ballistic) system, although it typically takes smaller values. We find a close relation between the behaviour of the entanglement entropy and the small- $q$  (long-wavelength) dependence of the momentum structure factor  $\mathcal{S}(q)$ .  $\mathcal{S}(q)$  increases linearly with  $q$  as in the homogeneous case, with a slope that grows with  $\mathcal{C}$ . In the presence of pairing, we find that even the addition of small anomalous terms affects very significantly the scaling of the entanglement entropy compared to the unpaired case. In particular, we focused on topological phase transitions for which the gap closes with either extended or critical multifractal states. In the former case, the scaling of the entanglement entropy mirrors the behaviour observed at the critical points of the homogeneous Kitaev chain, while in the latter, it shows only slight deviations arising at small length scales. In contrast with the unpaired case, we always observe  $\mathcal{C} \approx 1/6$  for different critical points, the known value for the homogeneous Kitaev chain with periodic boundary conditions.

## INTRODUCTION

The study of entanglement in many-body systems has been a great example of success where remarkable new insights were attained by applying concepts from quantum information theory to condensed matter systems. Among them, the universal scaling of the entanglement entropy in conformal critical points of one-dimensional systems stands out [1–4]. At these critical 1D systems, the entanglement entropy of a finite subsystem of an infinite system with  $N_A$  sites, scales as  $S = \mathcal{C} \log(N_A) + \text{cte}$ , where  $\mathcal{C} = c/3$  for systems with periodic boundary conditions (we refer below to systems with periodic boundaries unless otherwise stated) and  $c$  is the universal central charge of the corresponding conformal field theory. For a free fermion chain (that can be mapped to the XX model, through a Jordan-Wigner transformation),  $c = 1$ . On the other hand, at the critical points of the topological phase transitions in the Kitaev chain (or XY model), we have  $c = 1/2$ . In the presence of a gap, the entanglement entropy also scales logarithmically up to a length scale of the order of the inverse energy gap, above which it saturates. Given the universality of the entanglement entropy scaling, it does not depend on model details for a group of models that are all described by the same low-energy conformal field theory. This includes the addition of inhomogeneities such as disorder can therefore still lead to universal behaviour [5–10].

Other very interesting inhomogeneous systems for which entanglement has been less studied are quasiperiodic sys-

tems. These systems offer a wide range of exciting physics, from interesting localization properties [11–22] to topological features and edge physics [23–25]. Interest in quasiperiodic systems has been recently renewed due to progress in experiments in optical lattices [12, 14, 15, 26, 27] and metamaterials [13, 21, 23, 25, 28], and the increased focus on moiré systems [29, 30].

In one dimension, quasiperiodic systems host rich localization physics, transitions between extended ballistic phases with plane-wave-like eigenstates and localized phases, where the wave function is exponentially localized in real-space [11–15]. At the critical point, the eigenstates are multifractal both in real and momentum space. For some systems, non-fine-tuned phases with multifractal eigenstates can arise [31–38]. The entanglement entropy has been previously studied in quasiperiodic systems [39–44]. For the half-filled paradigmatic Aubry-André model [11], it was found to scale logarithmically with subsystem size at the extended phase and critical point, and to saturate in the localized phase at length scales larger than the localization length [41, 42, 45]. In the extended phase, the entanglement entropy was found to behave as in the homogeneous case, scaling with  $\mathcal{C} \approx 1/3$ . At the critical point, however, a different coefficient  $\mathcal{C} \approx 0.26$  was observed [42]. The entanglement entropy of a generalized Aubry-André model with long-range (power-law decaying) hoppings was also studied in Ref. [44], at half-filling. For some parameters, it was found that  $\mathcal{C} \neq 1/3$  even in the extended phase. In critical phases,  $\mathcal{C}$  was always found to be significantly lower. This raises the question on whether extended and critical phases can always be distinguished based on the scaling of the entanglement entropy. Moreover, a lot remains to explore on the behaviour of the entanglement en-

trophy in more generic regimes, including different fillings and different critical points and critical phases. In the presence of pairing, the entanglement entropy has not been studied so far on critical points, to our knowledge.

In this work, using numerically exact methods, we study the behaviour of the entanglement entropy in different classes of one-dimensional quasiperiodic systems both with and without pairing terms. We focus on multifractal critical points/phases and find that even though the entanglement entropy scales logarithmically with the subsystem size, apart from possible small oscillations, the coefficients  $\mathcal{C}$  depend significantly on the model parameters and electron filling in the absence of pairing. In fact, we observe that  $\mathcal{C} \approx 1/3$  at some critical points, with the entanglement entropy behaving similarly to the homogeneous case. Interestingly, the scaling of the entanglement entropy is closely related with the long-wavelength (low-energy) behaviour of the momentum structure factor  $\mathcal{S}(q)$ , growing linearly with  $q$ , with a slope that increases with  $\mathcal{C}$ .

To understand the impact of the pairing terms, we studied the quasiperiodic Kitaev chain, focusing on critical points of topological phase transitions. In this case, we found that the entanglement entropy behaves very similarly to the homogeneous Kitaev chain, where  $\mathcal{C} = 1/6$ , irrespectively of the model parameters. This is true no matter whether extended or multifractal states are present at the critical point, with the most significant deviations from the  $\mathcal{C} = 1/6$  behaviour only occurring for the latter case, at small length scales.

Our results show that while in the absence of pairing the scaling of the entanglement entropy can vary quite significantly in critical phases and even become very similar to the homogeneous case, the addition of pairing terms, even if small, is highly relevant and the scaling tends to become very similar to the homogeneous Kitaev critical chain at sufficiently large length scales.

## MODEL AND METHODS

*Models.*— We consider the following class of Hamiltonians,

$$\mathcal{H} = -t \sum_n (c_n^\dagger c_{n+1} + c_{n+1}^\dagger c_n) + \sum_n V_n c_n^\dagger c_n + \Delta \sum_n (c_n c_{n+1} + c_{n+1}^\dagger c_n^\dagger) \quad (1)$$

where  $c_n^\dagger$  creates an electron at site  $n$  and  $V_n$  will be considered to be either of the following quasiperiodic potentials:  $V_n^{(1)} = V \cos(2\pi\tau n + \phi) - \mu$  and  $V_n^{(2)} = \cos(2\pi\tau n + \phi)/[1 + \alpha \cos(2\pi\tau n + \phi)] - \mu$ . In the definitions of  $V_n$ ,  $\tau$  is an irrational number that we take to be  $\tau = (\sqrt{5} - 1)/2$ ,  $\phi$  is a (phase) shift in the quasiperiodic potential and  $\mu$  is the chemical potential. In what follows, energy will be measured in units of  $t$ . We will study three particular cases of the Hamiltonian in Eq. 1: the Aubry-André model ( $\Delta = 0$  and  $V_n^{(1)}$ ) [11], the Ganeshan-Pixley-Sarma (GPS) model,

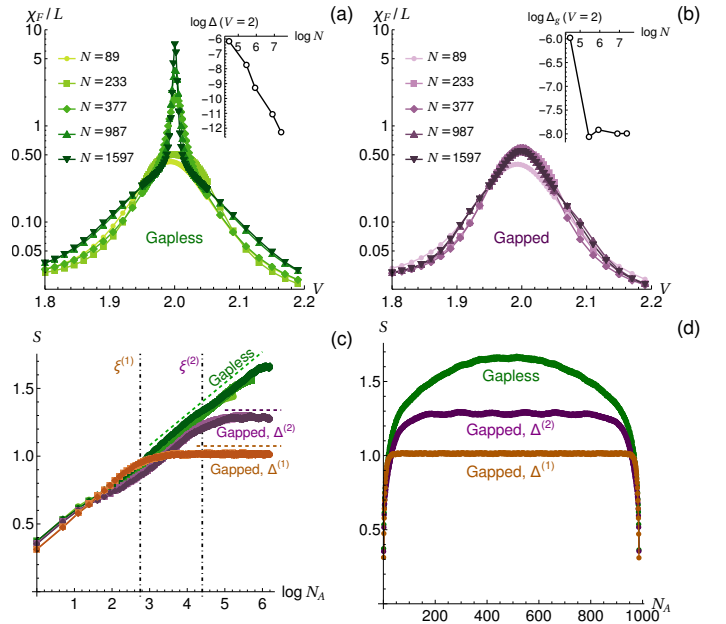


FIG. 1. Results for the Aubry-André model. (a,b)  $\chi_F/L$  at fillings  $\rho = 1/4$  (a) and  $\rho = \text{mod}(57\tau, 1)$  (b), for fixed twist  $\kappa = 1.7$  and  $\phi = 1.123/N$ . The insets show the energy gap as a function of system size for  $V = 2$ . (c) Entanglement entropy as a function of  $\log N_A$  up to  $N_A = N/2$  for  $V = 2$ , for  $\rho = 1/4$  (green),  $\rho^{(1)} = \text{mod}(10\tau, 1)$  (orange) and  $\rho^{(2)} = \text{mod}(57\tau, 1)$  (purple), and for system sizes  $N = \{377, 610, 987\}$  (respectively from lighter to darker color shade). Averages over  $N_c = 1800$  configurations were made. (d) Entanglement entropy for  $N_A \in [1, N]$ , for  $N = 987$ , for the same parameters as in (c).

with  $\Delta = 0$  and  $V_n^{(2)}$  [46], and the quasiperiodic Kitaev chain model,  $\Delta \neq 0$  with  $V_n^{(1)}$ . For the GPS model, the localization phase diagram is analytically known, hosting extended, localized and critical phases [46, 47]. For the quasiperiodic Kitaev chain, the localization and topological phase diagrams in the  $(V, \Delta)$  plane have also been explored [31, 33, 48, 49]. In particular, for  $\mu = 0$ , a topological phase transition between a topological phase with zero-energy majorana modes and a trivial phase takes place. At this critical point there is also a localization transition between phases with critical multifractal eigenstates (topological) and localized eigenstates (trivial).

In order to simulate finite systems we followed the usual procedure carried out for QPS [50–52]: for each size  $N = F_n$ , we take  $\tau$  to be a rational approximant of the inverse of the golden ratio,  $\tau = \tau_n = F_{n-1}/F_n$ , where  $F_n$  is the  $n$ -th Fibonacci number. Note that in this way the finite system is incommensurate (the system's unit cell for  $\tau = \tau_n$  has precisely  $N$  sites, the total system size) and we may apply periodic boundary conditions (PBC) without defects.

*Entanglement entropy and fidelity.*— We can write the quadratic fermionic Hamiltonian in Eq. 1 in the Nambu representation,

$$\mathcal{H} = \frac{1}{2} \mathbf{C}^\dagger \mathbf{H} \mathbf{C}, \quad \mathbf{H} = \begin{pmatrix} \mathbf{h} & \mathbf{\Delta} \\ \mathbf{\Delta}^\dagger & -\mathbf{h}^T \end{pmatrix} \quad (2)$$

, where  $\mathbf{C} = (c_1, \dots, c_N, c_1^\dagger, \dots, c_N^\dagger)^T$  is a Nambu vector and

$$\mathbf{h} = \begin{pmatrix} V_0 & -t & 0 & \dots & -t \\ -t & V_1 & -t & \dots & 0 \\ 0 & -t & \ddots & \dots & \vdots \\ \vdots & \vdots & \dots & V_{N-2} & -t \\ -t & 0 & \dots & -t & V_{N-1} \end{pmatrix} \quad (3)$$

$$\mathbf{\Delta} = \begin{pmatrix} 0 & \Delta & 0 & \dots & -\Delta \\ -\Delta & 0 & \Delta & \dots & 0 \\ 0 & -\Delta & \ddots & \dots & \vdots \\ \vdots & \vdots & \dots & 0 & \Delta \\ \Delta & 0 & \dots & -\Delta & 0 \end{pmatrix} \quad (4)$$

with these matrices satisfying  $\mathbf{h} = \mathbf{h}^\dagger$  and  $\mathbf{\Delta} = -\mathbf{\Delta}^T$ . The single-particle correlation matrix can then be defined as  $\chi = \text{tr}(Z^{-1} e^{-\beta \mathcal{H}} \mathbf{C} \mathbf{C}^\dagger) = \mathbb{I} - n_F(\mathbf{H})$ , where  $\beta$  is the inverse temperature,  $Z$  is the partition function and  $n_F$  is the Fermi-Dirac distribution. In order to compute the entanglement entropy, we consider our subsystem  $A$  to contain the first  $N_A$  sites of the full chain containing  $N$  sites. The entanglement entropy can then be computed as

$$S_A = -\text{Tr}[\chi_A \ln \chi_A], \quad \chi_A = [\chi]_{i,j \in \mathcal{A} \cup (\mathcal{A}+N)}, \quad (5)$$

where  $i, j$  are entries of matrix  $\chi$ ,  $\mathcal{A}$  is the set of site indexes of subsystem  $A$  and  $\mathcal{A}+N$  are the indices obtained by summing  $N$  to each of the site indices in  $\mathcal{A}$ .

In what follows, we average the results for the entanglement entropy over random uniformly distributed realizations of phase  $\phi$ , unless otherwise stated. For the calculations in the Aubry-André and GPS models, we also average over random twisted boundary conditions, by closing the boundaries with a phase twist  $e^{ik}$  ( $k = 0$  for PBC) [17]. We estimate the error bars of the average entanglement entropy through the error of the mean.

For a 1D critical system whose continuum limit is a conformal field theory, we have that [2, 3]

$$S = \mathcal{C} \log \left( \frac{N}{\pi} \sin(\pi N_A/N) \right) + \mathcal{C}', \quad (6)$$

where  $N_A$  is the number of sites in subsystem  $A$ , in which case the central charge of the conformal field theory is given by  $\mathcal{C}/3$ , for periodic boundary conditions. For  $N_A \ll N$  we therefore have  $S = \mathcal{C} \log N_A$ . For the homogeneous fermionic chain with no anomalous terms ( $V = \Delta = 0$ ), we have that

$\mathcal{C} = 1/3$ . For the Kitaev chain ( $V = 0, \Delta \neq 0$ ), on the other hand, we have that  $\mathcal{C} = 1/6$  because the central charge takes half the value of the homogeneous chain. For  $\Delta = 0$  and  $V \neq 0$ , the  $\mathcal{C} = 1/3$  scaling was found to hold for  $V$  within the extended phase [42] in the half-filled Aubry-André model. However, Ref. [44] found regimes where  $\mathcal{C}$  was smaller even for electron fillings within the extended phase for a long-range Aubry-André model, in the presence of multifractal to extended mobility edges. In the localized phase,  $S$  only grows logarithmically for  $N_A \lesssim \xi$ , where  $\xi$  is the localization length [42, 44, 45]. At critical points containing multifractal eigenstates,  $S$  was found to still scale logarithmically with  $N_A$ , although with significantly smaller  $\mathcal{C}$ , accompanied by possible log-periodic oscillations [53], as previously observed for aperiodic quantum spin chains [54, 55].

We will also compute the ground state fidelity, defined as [56, 57]

$$F(\Psi(\lambda), \Psi(\lambda')) = |\langle \Psi(\lambda) | \Psi(\lambda') \rangle|, \quad (7)$$

where  $|\Psi(\lambda)\rangle$  is the system's ground-state and  $\lambda$  is some selected parameter of the model. In the case of non-interacting fermions, the overlap in Eq. 7 can be simply computed through  $F(\Psi(\lambda), \Psi(\lambda')) = |\det(\Phi_\lambda^\dagger \Phi_{\lambda'})|$ , where  $\Phi_\lambda$  is a  $N \times M$  matrix containing the  $M$  filled single-particle eigenstates in its columns. Taking  $\lambda' = \lambda + \delta\lambda$ , we can compute the leading-order term of the fidelity as  $\delta\lambda \rightarrow 0$ . This term corresponds to the fidelity susceptibility  $\chi_F$ , which can be defined as [57, 58]

$$\chi_F = -\frac{\partial^2 F}{\partial(\delta\lambda)^2} = \lim_{\delta\lambda \rightarrow 0} \frac{-2 \log F}{(\delta\lambda)^2}. \quad (8)$$

In the following, we choose  $\delta\lambda$  small enough for  $\chi_F$  to be converged. The finite-size scaling of  $\chi_F$  can be used to tackle critical points and critical exponents. At a critical point, the maximum of  $\chi_F$ , typically scales super extensively and its maximizant approaches the critical point as the system size is increased [59].

*Localization probes.*— To inspect the localization properties, we compute inverse participation ratios (IPR). For each single-particle eigenstate  $|\psi_\alpha\rangle = \sum_n \psi_n^\alpha |n\rangle$ , where  $\{|n\rangle\}$  is a basis localized at each site (or the Nambu basis for  $\Delta \neq 0$ ), the generalized IPR is given by  $\text{IPR}_\alpha(q) = (\sum_n |\psi_n^\alpha|^2)^{-q} \sum_n |\psi_n^\alpha|^{2q}$  [60]. In general we have  $\text{IPR}_\alpha(q) \sim N^{-\tau(q)}$ , where  $\tau(q) = D_r(q)(q-1)$ . In the extended phase, we have  $D_r(q) = D$ , while in the localized phase the IPRs become  $L$ -independent for  $L$  sufficiently larger than the localization length and therefore  $D_r(q) = 0$ . Critical points/phases in 1D quasiperiodic systems have multifractal eigenstates, in which case  $D_r(q)$  is a non-linear function of  $q$ . For the quasiperiodic Kitaev chain, we also define a momentum space generalized IPR. In the diagonal basis defined as  $\gamma_\alpha = \sum_i u_{\alpha,i} c_i^\dagger + v_{\alpha,i} c_i$ , we define  $\tilde{u}_{\alpha,k} = L^{-1/2} \sum_j e^{2\pi j k/L} u_{\alpha,i}$  and  $\tilde{v}_{\alpha,k} = L^{-1/2} \sum_j e^{2\pi j k/L} v_{\alpha,i}$ . The momentum-space generalized IPR is then given by  $\text{IPR}_k(q) = \sum_k (|\tilde{u}_{\alpha,k}|^{2q} + |\tilde{v}_{\alpha,k}|^{2q}) \sim L^{-\tau_k(q)}$ . In this case,

we have  $\tau_k(q) = D_k(q)(q-1)$ , with  $D_k(q) = 0$  for ballistic extended states,  $D_k(q) = 1$  for localized states and  $D_k(q)$  is again a non-linear function of  $q$  for multifractal states. In what follows, we mostly compute the real-space IPR and set  $q = 2$ , unless otherwise stated, defining  $\text{IPR} = \text{IPR}(q = 2)$ .

*Topological invariant.*— Finally, in order to inspect topological properties of the quasiperiodic Kitaev chain, we make use of the topological invariant introduced in Ref. [49]. By writing the Hamiltonian in terms of two species of Majorana fermions, the equations of motion for zero energy Majorana modes can be written in terms of transfer matrices (see Appendix for details). The transfer matrix for one of the species of modes is defined, for a system of length  $N$ , as  $\mathcal{A}_N = \prod_{n=1}^N A_n$ , where  $A_n^{ij} = V_n/(\Delta+t)\delta_{i,0}\delta_{j,0} + (\Delta-t)/(\Delta+t)\delta_{i,0}\delta_{j,1} + \delta_{i,1}\delta_{j,0}$ . For the other species, the transfer matrix is  $B_n = \sigma_x A_n^{-1} \sigma_x$ . A topological invariant can then be defined as in Ref. [49],

$$\nu_T = -(-1)^{n_f}, \quad (9)$$

where  $n_f$  is the number of eigenvalues of  $\mathcal{A}_N$  with magnitude smaller than unity. Inside a topological phase  $\nu_T = -1$  ( $n_f = 0, 2$ ), while in a trivial phase  $\nu_T = 1$  ( $n_f = 1$ ).

*Structure factor.*— In order to compare the results for the entanglement entropy scaling with other physical observables, we also compute the momentum structure factor, defined as

$$\mathcal{S}(q) = N^{-1} \sum_{j,l} [\langle n_j n_l \rangle - \langle n_j \rangle \langle n_l \rangle] e^{iq(j-l)} \quad (10)$$

In the non-interacting limit that we study in this manuscript,  $\mathcal{S}(q)$  can be computed through

$$\mathcal{S}(q) = \frac{1}{N} \sum_{i,j=1}^N [(\Phi \Phi^\dagger)_{ii} \delta_{ij} - (|\Phi \Phi^\dagger|^2)_{ij}] e^{iq(i-j)} \quad (11)$$

where matrix  $\Phi$  was previously defined below Eq. 7. In gapless extended phases,  $\mathcal{S}(q)$  typically behaves as  $\mathcal{S}(q) = \frac{K}{2\pi} q$  at small  $q$  [61].

## RESULTS

### Aubry-André and GPS models

We start by analysing the Aubry-André model. Some care is needed when computing the entanglement entropy, since energy gaps are known to open at commensurate fillings  $\rho_n = \text{mod}(n\tau, 1)$ ,  $n \in \mathbb{Z}$  [62, 63]. In fact, by applying perturbation theory in the quasiperiodic potential with respect to the homogeneous system, one finds that a gap is opened at filling  $\rho_n$  at order  $|n|$  in perturbation theory and therefore the gap size typically decreases with  $|n|$ . While in the extended phase, gaps can only be effectively opened for  $|n| \lesssim \xi$ , where  $\xi$  is the correlation length

( $\xi = 1/\log(2/V)$  in the extended phase for the Aubry-André model [11]), at critical points/phases  $\xi$  diverges and gaps can open at any order. For a finite system, we cannot get arbitrarily close to an incommensurate filling and we may end up choosing a (gapped) commensurate filling for some sizes. In order to try to avoid this problem we (i) start by choosing a number  $N'_p = \lfloor \rho N \rfloor$  of filled states, where  $\lfloor x \rfloor$  rounds  $x$  to the nearest integer; (ii) compute the energy gaps  $\Delta_g^0 = \epsilon(N'_p) - \epsilon(N'_p - 1)$  and  $\Delta_g^1 = \epsilon(N'_p + 1) - \epsilon(N'_p)$ , where  $\epsilon(N_p)$  is the single-particle eigenenergy of the  $N_p$ -th eigenstate, and choose the final number of filled states to be  $N_p = N'_p - 1 + \arg \min_j \{\Delta_g^j\}$ ,  $j = 0, 1$ . In this way, by always choosing the smallest gap closer to the chosen filling  $\rho$  we minimize the risk of accidentally coming across a commensurate filling for a given system. In Fig. 1 we show the results for the fidelity susceptibility and entanglement entropy obtained by carrying out the procedure just described for the Aubry-André model, at quarter-filling ( $\rho = 1/4$ ), comparing with the results for a close commensurate filling  $\rho_{57} = \text{mod}(57\tau, 1) \approx 0.228$ . In Fig. 1(a) we find true criticality since  $\chi_F$  is superextensive at the critical point. This arises from the gapless nature of the chosen filling, as can be seen by the decreasing of the energy gap,  $\Delta_g$ , with  $N$  at the critical point [inset of Fig. 1(a)]. For the commensurate filling, the system is gapped as can be seen by the convergence of  $\Delta_g$  in  $N$ , in the inset of Fig. 1(b). Even though this gap is quite small, we can see that there is clearly no divergence in  $\chi_F/N$  for a sufficiently large system size at the critical point. In this case, the system is always gapped, even at the critical point, which gives rise to an avoided criticality. These qualitative differences naturally manifest in the scaling of the entanglement entropy, as shown in Figs. 1(c,d). While in the gapless case, it scales as  $\log N_A$  for  $N_A \ll N$ , only saturating at extensively larger length scales  $\Lambda \simeq N/2$  (see Eq. 6), in the gapped case, it only grows up to a  $N$ -independent length scale  $\xi_g$ , inversely proportional to the gap size. In Figs. 1(c,d) we also compare the results for fillings  $\rho^{(1)} = \rho_{10}$  and  $\rho^{(2)} = \rho_{57}$ , where we clearly see that  $S$  saturates for  $N_A \gtrsim \xi^{(1)}$  and  $N_A \gtrsim \xi^{(2)} > \xi^{(1)}$  since  $\Delta^{(1)} > \Delta^{(2)}$ .

From this point on we focus on incommensurate/gapless fillings. In Fig. 2(a) we compute the entanglement entropy for the quarter-filled Aubry-André model, and for  $V$  close to the critical point. At the critical point we see that  $S$  scales as  $\log N_A$  with  $\mathcal{C} \approx 0.23$ , slower than in the homogeneous system. Interestingly, close to the critical point we see that  $S$  closely follows the critical behaviour for length scales  $N_A \lesssim \xi$ , where  $\xi$  is the correlation length ( $\xi = 1/\log(2/V)$  in the extended phase, while  $\xi = 1/\log(V/2)$  in the localized phase). For  $N_A \gtrsim \xi$ , we see a crossover to a scaling with  $\mathcal{C} = 1/3$  in the extended phase, as in the homogeneous case, while there is a saturation in the localized phase. In Fig. 2(b), we compute the scaling of  $S$  in different critical points/phases, comparing with the results obtained deep in the extended phase. We see that the scaling of  $S$  in the critical phase can vary significantly, and even closely resemble the homogeneous/extended scaling. This is in contrast



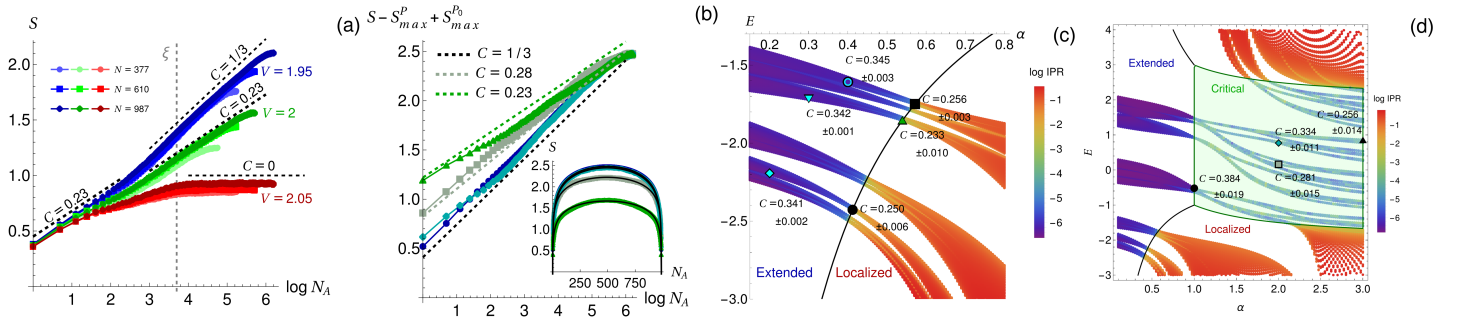


FIG. 2. (a) Entanglement entropy  $S$  for the Aubry-André model, for filling  $\rho = 1/4$ . The blue, green and red data points correspond to  $V = 1.95$  (extended),  $V = 2$  (critical) and  $V = 2.05$  (localized), respectively. The dashed lines are guides to the eye for the scaling of the entanglement entropy. The gray dashed line indicates  $\log \xi = 2.7$ , where  $\xi$  is approximately the exact correlation length for  $V = 1.95$  ( $\xi = 1/\log(2/V)$ ) and  $V = 2$  ( $\xi = 1/\log(V/2)$ ). (b)  $S$  for different critical points [ $V = 1, \alpha = 2, \rho = 0.47$  (green);  $V = 1, \alpha = 2, \rho = 0.538$  (light blue);  $V = 1, \alpha = 0.539, \rho = 0.25$  (gray)] and an extended point ( $\rho = 0.25, \alpha = 0, V = 1$ ).  $S$  was shifted so that the maxima coincide for all the analysed points, where  $P_0$  is the extended point and  $P$  is the point being analysed. These points are signaled in (c,d), with the plot markers matching the ones in this figure. The dashed lines show the slopes  $C$  obtained by fitting  $S$  to Eq. 6 for all  $N_A$ , where the fits are shown in the inset. (c) IPR for the GPS model around an extended-to-localized transition, for  $L = 987$  and  $V = 1$ , along with fitting results for  $C$  at different points. The black line denotes the analytical mobility edge between the extended and localized phases. (d) IPR for the same model, in a range of parameters containing the critical phase, together with the value of  $C$  extracted from the fit within this phase. The error bars correspond to the standard deviation of the fitted  $C$  for the three larger considered sizes,  $N = \{610, 987, 1597\}$ . For all the calculations of the entanglement entropy in (a-d), we averaged over 1800 configurations of shifts and twists for  $N = \{377, 610, 987\}$  and 252 configurations for  $N = 1597$ .

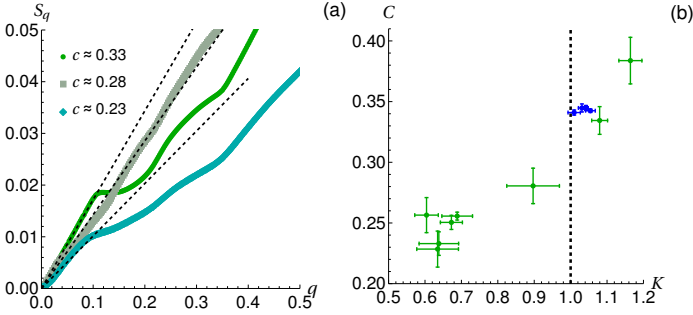


FIG. 3. (a) Structure factor  $S(q)$  for the same critical points analysed in Fig. 2, with the corresponding values of  $C$  indicated in the legend. The black dashed lines correspond to the  $S(q) = Kq/(2\pi)$ , with the  $K$  computed in (b) for the corresponding critical point. (b)  $C$  vs.  $K$  for the different critical (green) and extended (blue) points studied in Fig. 2.  $K$  was computed through  $K = 2\pi S(\delta q)/\delta q$ , with  $\delta q = 20\pi/N$  and for a fixed random configuration of  $\kappa$  and  $\phi$  (the results of  $S(q)$  depend very weakly on  $\kappa$  and  $\phi$ ). The error bars correspond to the standard deviation of the obtained results for the system sizes  $N = \{1597, 2584, 4181\}$ . The extended points are clustered close to  $K = 1$ , marked with the vertical dashed line.

with previous results obtained for the Aubry-André model with long-range hoppings for which  $C$  was always found to be significantly lower than in the homogeneous or extended case, when the fillings were chosen in regions of multifractal eigenstates. We also note that even though  $S$  grows with  $\log N_A$ , it also shows small oscillations. These oscillations are expected: in fact log-periodic oscillations were previously found at the critical point of the half-filled Aubry-André model with  $\tau = 1/\sqrt{2}$  [53] and also in aperiodic spin

chains [54, 55]. In Figs. 2(c,d), we compute  $C$  at localization-delocalization transitions (c) and inside the critical phase (d) by fitting  $S(N_A)$  to Eq. 6. We find that  $C$  can take a wide range of non-universal values. Interestingly, for localization-delocalization transitions at filling  $\rho = 1/4$  we find that the scaling of the entanglement entropy for the Aubry-André and GPS models is compatible, in agreement with the critical point universality proposed in Ref. [53]. This again suggests that at extended-localized transitions the behaviour of entanglement entropy is universal for significantly different models at fixed fillings, as conjectured in Ref. [53].

We now try to establish a connection between the scaling of  $S$  and other physical properties. At critical points, correlation functions of the type  $\langle \mathcal{O}_i \mathcal{O}_j \rangle$  are expected to decay in a power-law fashion as  $\langle \mathcal{O}_i \mathcal{O}_{i+\epsilon} \rangle \sim |\epsilon|^{-y_0}$  for large enough  $|\epsilon|$ . Taking the simplest correlation function,  $\langle c_i^\dagger c_{i+\epsilon} \rangle$ , we find that  $\langle c_i^\dagger c_{i+\epsilon} \rangle \sim |\epsilon|^{-1}$  in the extended phase with the interesting possible formation of moiré patterns (see Appendix ); while in the localized phase  $\langle c_i^\dagger c_{i+\epsilon} \rangle \sim e^{-|\epsilon|/\xi}$ , where  $\xi$  is the localization length. At critical phases/points, however, there are very large fluctuations as function of  $\epsilon$  and it becomes challenging to define the power-law exponent. In fact, the scaling of the maxima of these fluctuations is compatible with  $|\epsilon|^{-1}$ . Therefore, no significant distinctions in the scalings of  $g_r(\epsilon)$  were found in the critical regions. The connection between  $S$  and the general behaviour of correlation functions is therefore more subtle. In fact, a clear relation between the entanglement entropy and the low-momentum scaling of the structure factor  $S(q)$ , given in Eq. 10, can be found. In Fig. 3(a) we can see that only the slope of the scaling,  $K$  (see below Eq. 10), changes at critical points, while the linear scaling in  $q$  still holds as in the extended phase,

up to small oscillations. By computing  $K$  for the different critical and extended points that we studied in Fig. 2, and comparing the results with  $\mathcal{C}$ , we verified that  $K$  increases with  $\mathcal{C}$  as shown in Fig. 3(b). While at extended points we have  $K \approx 1$  (blue points in Fig. 3) as in the homogeneous case, in the critical case the values of  $K$  can vary significantly.

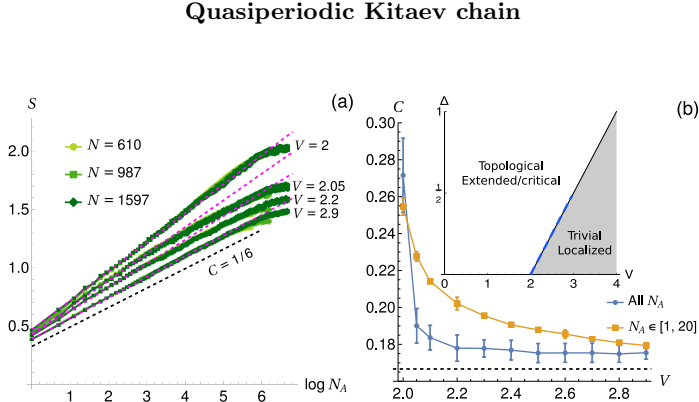


FIG. 4. (a)  $S$  for the quasiperiodic Kitaev chain, for  $\mu = 0$  and different  $(V, \Delta)$  across the topological transition shown in the inset of (b), given by  $\Delta(V) = V/2 - 1$ . The values of  $V$  are indicated close to the corresponding curves. The dashed magenta lines correspond to linear fits made for  $N_A \leq 20$ . (b)  $\mathcal{C}$  obtained by fitting  $S$  to Eq. 6 for all  $N_A$  (blue) and by making a linear fit of the  $(\log N_A, S)$  data only for  $N_A \leq 20$  (yellow). The data points were computed by averaging the results obtained for the system sizes  $N = \{610, 987, 1597\}$  and the error bars correspond to the standard deviation. The inset contains the topological phase diagram in the  $(V, \Delta)$  plane. The blue dashed line in the inset indicates the explored range of the critical line.

The quasiperiodic Kitaev chain has a well-known phase diagram in the  $\Delta - V$  plane for  $\mu = 0$  [31], shown in the inset of Fig. 4 (see also Ref. [33] for full localization phase diagram and Ref. [64] for exact analytical solution). Here we computed the entanglement entropy at the critical line of the transition between a topological phase with critical eigenstates, having majorana zero modes, and a trivial localized phase. The results for  $\mathcal{C}$  are shown in Fig. 4. For  $(V, \Delta) = (2, 0)$ ,  $\mathcal{C}$  has the value of the Aubry-André critical point ( $\mathcal{C} \approx 0.26$  at half-filling [42]). However, for finite  $\Delta$ ,  $\mathcal{C}$  quickly becomes smaller, getting close to the homogeneous Kitaev chain’s value,  $\mathcal{C} = 1/6$ , with the most significant deviations arising only at small  $N_A$ . This can be observed by fitting the scaling of the entanglement entropy at small  $N_A$  - Fig. 4(b) - for which we see a significant  $V$ -dependence. When fitting  $S$  to Eq. 6 using all  $N_A$ , we found that  $\mathcal{C}$  is essentially constant for different critical points of the transition, in contrast to the critical points of the unpaired models, for which  $\mathcal{C}$  varied significantly.

In order to understand whether the almost constant value of  $\mathcal{C}$  was a special feature of the analysed transition, we also studied the  $\mu \neq 0$  case. In this case we can have reentrant topological transitions, similar to what is observed for topo-

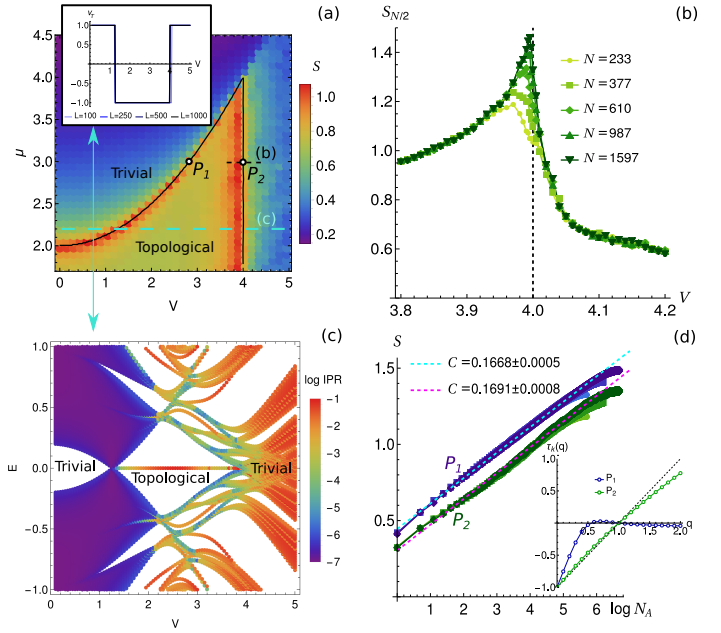


FIG. 5. Results for  $\Delta = 1$ . (a)  $S$  for  $N = 233$  and  $N_A = [N/6]$ , with each point corresponding to an average over 75 realizations. The full black line shows the phase boundaries obtained through the topological invariant in Eq. 9. The inset show the results for this topological invariant at a fixed  $\mu$  cut ( $\mu = 2.2$ ) marked by the cyan dashed line. (b) Finite-size scaling of  $S$  for variable  $N$  and  $N_A = [N/2]$ . We averaged over  $N_c = 1800$  configurations for  $N \leq 987$  and  $N_c = 252$  for  $N = 1597$ . (c) IPR results for  $N = 987$ , with open boundary conditions, and for parameters at the cyan dashed cut in (a). (d)  $S$  at critical points  $P_1$  and  $P_2$  indicated in (a). The lighter, intermediate and darker colors correspond respectively to  $N = 610, 987, 1597$ , with the results respectively averaged over  $N_c = 1800, 1800, 252$  configurations. The inset contains the results for the multifractal exponent  $\tau_k(q)$ , computed by fitting  $\text{IPR}_k(q)$  for  $N \in [144, 2584]$ . We used  $N_c \in [25 - 725]$  configurations of  $\phi$  for  $P_2$  and a single random configuration for  $P_1$  (the  $\phi$ -dependence is negligible in this case). We note that for  $P_1$ ,  $\tau_k(q)$  deviates significantly from 0 for small  $q$ , which we attribute to finite-size effects.

logical Anderson insulators, in the disordered case [65, 66]. This is shown in Fig. 5(a) for  $\Delta = 1$ . In this figure, we can see that we can start in a trivial phase, at  $\mu > 2$ , and transition into a topological phase by increasing  $V$ . The topological phase contains zero-energy modes as expected, which we illustrate in Fig. 5(c). At an even larger value of  $V$ , we have a new topological transition back into a trivial phase. These two topological transitions are however of different nature in terms of localization properties. Exactly at the transition point the eigenstates are ballistic in the first and multifractal in the second. This is shown in the inset of Fig. 5(d), where we plotted  $\tau_k(q)$  for examples of these transitions, at points  $P_1$  and  $P_2$ , indicated in Fig. 5(a). We can see, however, that the scaling of the entanglement entropy is similar for both transitions, apart from the existence of oscillations in the critical case, as in the other studied critical points.

## DISCUSSION

In this work, we characterized in detail the entanglement entropy in different models of one-dimensional fermionic quasiperiodic systems, focusing on multifractal critical points/phases. In the absence of pairing, we found that the entanglement entropy follows the expected behaviour for one-dimensional critical systems, but can show possible small oscillations. Similar log-periodic oscillations were previously found in Ref. [54, 55] for aperiodic spin chains and in Ref. [53] both for the non-interacting and interacting Aubry-André model. In the absence of pairing, we found that the characteristic coefficient  $\mathcal{C}$  that governs the scaling of the entanglement entropy with subsystem size  $N_A$  and total size  $N$  depends significantly on the model parameters and electron filling. At some critical points, we observed that the entanglement entropy even behaves similarly to the homogeneous case, with  $\mathcal{C} \approx 1/3$ . This is in contrast with previous studies where  $\mathcal{C}$  was always found to be significantly smaller at critical multifractal phases/points, compared to the homogeneous case [42, 44]. Although there are significant variations of  $\mathcal{C}$ , we find that compatible values are obtained for the Aubry-André and GPS models at critical points of localization-delocalization transitions, for a fixed filling. This is in agreement with Ref. [53], where a universal behaviour of the entanglement entropy was found at the localization transitions of different half-filled quasiperiodic chains. We also compared the behaviour of the entanglement entropy with correlation functions and found that  $\mathcal{C}$  was closely related with the long-wavelength behaviour of the momentum structure factor.

For critical quasiperiodic Kitaev chains, we found that the addition of even small pairing terms is highly relevant for the behaviour of the entanglement entropy. Independently of studied critical points, we find that it behaves similarly to the homogeneous critical Kitaev chain, where  $\mathcal{C} = 1/6$ , departing from the non-universal larger values of  $\mathcal{C}$  computed in the unpaired case. The most significant deviations from  $\mathcal{C} = 1/6$  only occur at small length scales, when the critical point contains multifractal eigenstates.

Future interesting studies include to address the impact of interactions on the entanglement entropy, in critical phases with multifractal eigenstates. In Ref. [53], short-range spinless interactions were found to be irrelevant at critical points between extended and localized phases, so we expect that our results at these transitions also hold in the interacting case. However, interactions can be relevant in multifractal critical phases of quasiperiodic systems [67], which may change the behaviour of the entanglement entropy.

- 
- [1] G. Vidal, J. I. Latorre, E. Rico, and A. Kitaev, *Phys. Rev. Lett.* **90**, 227902 (2003).  
 [2] P. Calabrese and J. Cardy, *Journal of Statistical Mechanics: Theory and Experiment* **2004**, P06002 (2004).  
 [3] P. Calabrese and J. Cardy, *Journal of Physics A: Mathematical*

- ical and Theoretical* **42**, 504005 (2009).  
 [4] L. Amico, R. Fazio, A. Osterloh, and V. Vedral, *Rev. Mod. Phys.* **80**, 517 (2008).  
 [5] G. Refael and J. E. Moore, *Phys. Rev. Lett.* **93**, 260602 (2004).  
 [6] A. Saguia, M. S. Sarandy, B. Boechat, and M. A. Continentino, *Phys. Rev. A* **75**, 052329 (2007).  
 [7] G. Refael and J. E. Moore, *Journal of Physics A: Mathematical and Theoretical* **42**, 504010 (2009).  
 [8] M. Pouranvari and K. Yang, *Phys. Rev. B* **89**, 115104 (2014).  
 [9] I. Mondragon-Shem and T. L. Hughes, *Phys. Rev. B* **90**, 104204 (2014).  
 [10] Y. Mohdeb, J. Vahedi, N. Moure, A. Roshani, H.-Y. Lee, R. N. Bhatt, S. Kettemann, and S. Haas, *Phys. Rev. B* **102**, 214201 (2020).  
 [11] S. Aubry and G. André, Proceedings, VIII International Colloquium on Group-Theoretical Methods in Physics **3** (1980).  
 [12] G. Roati, C. D’Errico, L. Fallani, M. Fattori, C. Fort, M. Zaccanti, G. Modugno, M. Modugno, and M. Inguscio, *Nature* **453**, 895 (2008), arXiv:0804.2609.  
 [13] Y. Lahini, R. Pugatch, F. Pozzi, M. Sorel, R. Morandotti, N. Davidson, and Y. Silberberg, *Physical Review Letters* (2009), 10.1103/PhysRevLett.103.013901.  
 [14] M. Schreiber, S. S. Hodgman, P. Bordia, H. P. Lüschen, M. H. Fischer, R. Vosk, E. Altman, U. Schneider, and I. Bloch, *Science* **349**, 842 (2015), arXiv:1501.05661.  
 [15] H. P. Lüschen, S. Scherg, T. Kohlert, M. Schreiber, P. Bordia, X. Li, S. Das Sarma, and I. Bloch, *Physical Review Letters* (2018), 10.1103/PhysRevLett.120.160404.  
 [16] C. Huang, F. Ye, X. Chen, Y. V. Kartashov, V. V. Konotop, and L. Torner, *Scientific Reports* **6**, 32546 (2016).  
 [17] J. H. Pixley, J. H. Wilson, D. A. Huse, and S. Gopalakrishnan, *Phys. Rev. Lett.* **120**, 207604 (2018).  
 [18] M. J. Park, H. S. Kim, and S. Lee, *Phys. Rev. B* **99**, 245401 (2019), arXiv:1812.09170.  
 [19] B. Huang and W. V. Liu, *Phys. Rev. B* **100**, 144202 (2019).  
 [20] Y. Fu, E. J. König, J. H. Wilson, Y.-Z. Chou, and J. H. Pixley, *npj Quantum Materials* **5**, 71 (2020).  
 [21] P. Wang, Y. Zheng, X. Chen, C. Huang, Y. V. Kartashov, L. Torner, V. V. Konotop, and F. Ye, *Nature* (2020), 10.1038/s41586-019-1851-6, arXiv:2009.08131.  
 [22] M. Gonçalves, H. Z. Olyaei, B. Amorim, R. Mondaini, P. Ribeiro, and E. V. Castro, “Incommensurability-induced sub-ballistic narrow-band-states in twisted bilayer graphene,” (2020), arXiv:2008.07542 [cond-mat.mes-hall].  
 [23] Y. E. Kraus, Y. Lahini, Z. Ringel, M. Verbin, and O. Zeitlinger, *Physical Review Letters* (2012), 10.1103/PhysRevLett.109.106402, arXiv:1109.5983.  
 [24] Y. E. Kraus and O. Zeitlinger, *Phys. Rev. Lett.* **109**, 116404 (2012).  
 [25] M. Verbin, O. Zeitlinger, Y. E. Kraus, Y. Lahini, and Y. Silberberg, *Physical Review Letters* (2013), 10.1103/PhysRevLett.110.076403, arXiv:1211.4476.  
 [26] D. J. Boers, B. Goedeke, D. Hinrichs, and M. Holthaus, *Phys. Rev. A* **75**, 63404 (2007).  
 [27] M. Modugno, *New Journal of Physics* **11**, 33023 (2009).  
 [28] M. Verbin, O. Zeitlinger, Y. Lahini, Y. E. Kraus, and Y. Silberberg, *Phys. Rev. B* **91**, 64201 (2015).  
 [29] L. Balents, C. R. Dean, D. K. Efetov, and A. F. Young, *Nat. Phys.* **16**, 725 (2020).  
 [30] E. Y. Andrei, D. K. Efetov, P. Jarillo-Herrero, A. H. MacDonald, K. F. Mak, T. Senthil, E. Tutuc, A. Yazdani, and A. F. Young, *Nature Reviews Materials* **6**, 201 (2021).  
 [31] W. DeGottardi, D. Sen, and S. Vishveshwara, *Phys. Rev. Lett.* **110**, 146404 (2013).

- [32] F. Liu, S. Ghosh, and Y. D. Chong, *Phys. Rev. B - Condens. Matter Mater. Phys.* **91**, 014108 (2015).
- [33] J. Wang, X.-J. Liu, G. Xianlong, and H. Hu, *Phys. Rev. B* **93**, 104504 (2016).
- [34] X. Deng, S. Ray, S. Sinha, G. V. Shlyapnikov, and L. Santos, *Phys. Rev. Lett.* **123**, 025301 (2019).
- [35] Y. Wang, L. Zhang, S. Niu, D. Yu, and X.-J. Liu, *Phys. Rev. Lett.* **125**, 073204 (2020).
- [36] T. Čadež, R. Mondaini, and P. D. Sacramento, *Physical Review B* (2019), 10.1103/PhysRevB.99.014301, arXiv:1808.10238.
- [37] T. Liu, X. Xia, S. Longhi, and L. Sanchez-Palencia, *SciPost Phys.* **12**, 27 (2022).
- [38] M. Gonçalves, B. Amorim, E. V. Castro, and P. Ribeiro, “Critical phase dualities in 1d exactly-solvable quasiperiodic models,” (2023), arXiv:2208.07886 [cond-mat.dis-nn].
- [39] X. Li, J. H. Pixley, D.-L. Deng, S. Ganeshan, and S. Das Sarma, *Phys. Rev. B* **93**, 184204 (2016).
- [40] N. Roy and A. Sharma, *Phys. Rev. B* **100**, 195143 (2019).
- [41] P. Ribeiro, M. Haque, and A. Lazarides, *Phys. Rev. A* **87**, 043635 (2013).
- [42] G. m. H. Roósz, Z. Zimborás, and R. Juhász, *Phys. Rev. B* **102**, 064204 (2020).
- [43] R. Ghosh and A. Das, *Phys. Rev. B* **103**, 024202 (2021).
- [44] N. Roy and A. Sharma, *Phys. Rev. B* **103**, 075124 (2021).
- [45] N. Roy and A. Sharma, *Phys. Rev. B* **97**, 125116 (2018).
- [46] S. Ganeshan, J. H. Pixley, and S. Das Sarma, *Phys. Rev. Lett.* **114**, 146601 (2015).
- [47] T. Liu, X. Xia, S. Longhi, and L. Sanchez-Palencia, arXiv e-prints, arXiv:2105.04591 (2021), arXiv:2105.04591 [cond-mat.dis-nn].
- [48] X. Cai, L.-J. Lang, S. Chen, and Y. Wang, *Phys. Rev. Lett.* **110**, 176403 (2013).
- [49] W. DeGottardi, D. Sen, and S. Vishveshwara, *New Journal of Physics* **13**, 065028 (2011).
- [50] M. Y. Azbel, *Phys. Rev. Lett.* **43**, 1954 (1979).
- [51] A. Szabó and U. Schneider, *Physical Review B* (2018), 10.1103/PhysRevB.98.134201, arXiv:1803.09756.
- [52] Y. Wang, X. Xia, L. Zhang, H. Yao, S. Chen, J. You, Q. Zhou, and X. J. Liu, *Phys. Rev. Lett.* **125**, 196604 (2020), arXiv:2004.11155.
- [53] M. Gonçalves, J. H. Pixley, B. Amorim, E. V. Castro, and P. Ribeiro, “Short-range interactions are irrelevant at the quasiperiodic-driven luttinger liquid to anderson glass transition,” (2023), arXiv:2304.09197 [cond-mat.dis-nn].
- [54] R. Juhász and Z. Zimborás, *Journal of Statistical Mechanics: Theory and Experiment* **2007**, P04004 (2007).
- [55] F. Igloi, R. Juhász, and Z. Zimborás, *Europhysics Letters* **79**, 37001 (2007).
- [56] P. Zanardi and N. Paunković, *Phys. Rev. E* **74**, 031123 (2006).
- [57] S.-J. GU, *International Journal of Modern Physics B* **24**, 4371 (2010), <https://doi.org/10.1142/S0217979210056335>.
- [58] W.-L. You, Y.-W. Li, and S.-J. Gu, *Phys. Rev. E* **76**, 022101 (2007).
- [59] S.-J. GU, *International Journal of Modern Physics B* **24**, 4371 (2010), <https://doi.org/10.1142/S0217979210056335>.
- [60] C. Aulbach, A. Wobst, G.-L. Ingold, P. Hänggi, and I. Varga, *New Journal of Physics* **6**, 70 (2004).
- [61] In a Luttinger liquid phase,  $K$  is the Luttinger liquid correlation parameter.
- [62] B. Bernevig and T. Hughes, *Topological Insulators and Topological Superconductors* (Princeton University Press, 2013).
- [63] T. Cookmeyer, J. Motruk, and J. E. Moore, *Phys. Rev. B* **101**, 174203 (2020).
- [64] M. Gonçalves, B. Amorim, E. V. Castro, and P. Ribeiro, *Phys. Rev. B* **108**, L100201 (2023).
- [65] J. Li, R.-L. Chu, J. K. Jain, and S.-Q. Shen, *Phys. Rev. Lett.* **102**, 136806 (2009).
- [66] L. Levy and M. Goldstein, *Universe* **5** (2019), 10.3390/universe5010033.
- [67] M. Gonçalves, B. Amorim, F. Riche, E. V. Castro, and P. Ribeiro, “Incommensurability enabled quasi-fractal order in 1d narrow-band moiré systems,” (2023), arXiv:2305.03800 [cond-mat.str-el].
- [68] We note that even though  $\kappa_F$  is only well-defined for  $V = 0$ ,  $n_\kappa$  still shows a sharp decrease at  $\kappa = \kappa_F$  in the extended (and even critical) phase of the Aubry-André model.



## Quasiperiodic Kitaev chain: clean limit and topological properties

In this section, we provide additional details on how the topological properties of the quasiperiodic Kitaev chain were studied in the main text. For  $V = 0$ , this model is homogeneous and exhibits a phase transition at  $|\mu| = |t|$ , for any  $\Delta$  [49]. At this point, the entanglement entropy scales with  $\mathcal{C} = 1/6$  [1]. Otherwise, the system is gapped and the entanglement entropy saturates for large enough  $N_A$ . We reproduce these results, in Fig. 6.

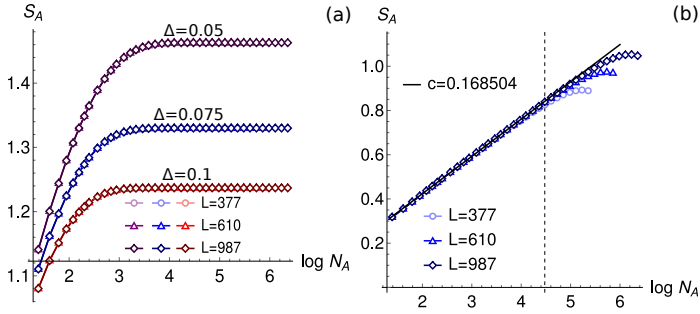


FIG. 6. (a) Entanglement entropy for the homogeneous Kitaev chain, for  $\mu = 0$  and variable  $\Delta$ . Note that the energy gap increases with  $\Delta$ . Therefore, for larger  $\Delta$ ,  $S$  saturates for smaller  $N_A$ , of the order of the inverse gap. (b) Entanglement entropy for the clean Kitaev chain, for  $\Delta = 0.1, \mu = 2$  (critical point).  $S_A$  scales with the correct pre-factor  $\mathcal{C} \approx 1/6$  consistent with the central charge  $c = 1/2$  of the Kitaev model.

In order to study the topological properties of the model, in particular for the phase diagram in Fig. 5(a), we used a topological invariant first defined in Ref. [49]. We now provide some additional details on this quantity. Let us introduce the Majorana fermions  $a_n$  and  $b_n$  such that  $c_n = (a_n + ib_n)/2$ .  $a_n$  and  $b_n$  satisfy  $\{a_n, b_n\} = 0$  and  $\{a_n, a_m\} = \{b_n, b_m\} = 2\delta_{mn}$  (and therefore  $a_n^2 = b_n^2 = 1$ ). The Hamiltonian for the quasiperiodic Kitaev chain becomes:

$$H = \frac{i}{2} \sum_n \left( (-t + \Delta)a_n b_{n+1} + (t + \Delta)b_n a_{n+1} + [V \cos(2\pi\tau n + \phi) - \mu]a_n b_n \right) + \text{cte} \quad (12)$$

The Majorana zero modes are represented by the operators  $\Gamma_a = \sum_n \alpha_n a_n$  and  $\Gamma_b = \sum_n \beta_n b_n$ , whose amplitudes  $\alpha_n$  and  $\beta_n$  satisfy the zero-energy equations of motion for the Hamiltonian in Eq. 12:

$$\begin{aligned} (t - \Delta)\alpha_{n-1} + (t + \Delta)\alpha_{n+1} - V_n \alpha_n &= 0 \\ -(t + \Delta)\beta_{n-1} - (t - \Delta)\beta_{n+1} + V_n \beta_n &= 0 \end{aligned} \quad (13)$$

where  $V_n = V \cos(2\pi\tau n + \phi) - \mu$ . We can write these decoupled equations in the transfer matrix form:

$$\begin{pmatrix} \alpha_{n+1} \\ \alpha_n \end{pmatrix} = A_n \begin{pmatrix} \alpha_n \\ \alpha_{n-1} \end{pmatrix}, \quad A_n = \begin{pmatrix} \frac{V_n}{\Delta+t} & \frac{\Delta-t}{\Delta+t} \\ 1 & 0 \end{pmatrix} \quad (14)$$

$$\begin{pmatrix} \beta_{n+1} \\ \beta_n \end{pmatrix} = B_n \begin{pmatrix} \beta_n \\ \beta_{n-1} \end{pmatrix}, \quad B_n = \sigma_x A_n^{-1} \sigma_x \quad (15)$$

where  $\sigma_x$  is a Pauli matrix. Considering a semi-infinite chain starting at site  $n = 1$ , we have  $\alpha_0 = \beta_0 = 0$ . At site  $n = N + 1$  we have

$$\begin{pmatrix} \alpha_{N+1} \\ \alpha_N \end{pmatrix} = \mathcal{A}_L \begin{pmatrix} \alpha_1 \\ 0 \end{pmatrix}, \quad \mathcal{A}_N = \prod_{n=1}^N A_n \quad (16)$$

In the same way, we can define

$$\mathcal{B}_N = \prod_{n=1}^N B_n \quad (17)$$

In order to have Majorana modes localized at the edges of the chain, both the eigenvalues of  $\mathcal{A}_N$  should be either smaller or larger than one in magnitude as  $N \rightarrow \infty$ . In the former case, we have a localized  $a$ -mode, while in the latter, we have a localized  $b$ -mode (at the left boundary). If only one of the eigenvalues of  $\mathcal{A}_N$  is larger than unity, then both the  $a$ - and  $b$ -modes are not normalizable and we cannot have localized Majorana modes.

Based on these considerations we can define a topological invariant as in Ref. [49]:

$$\nu_T = -(-1)^{n_f} \quad (18)$$

where  $n_f$  is the number of eigenvalues with magnitude smaller than unity. For  $n_f = 0, 2$ ,  $\nu_T = -1$  and the phase is topological. For  $n_f = 1$ ,  $\nu_T = 1$  and the phase is trivial.

### Single-particle correlation matrix in the Aubry-André model

We finally provide additional results on single-particle correlation functions for the Aubry-André model. We define the real and momentum-space single-particle correlation matrices as

$$\chi_{rr'} = \langle c_r^\dagger c_{r'} \rangle \quad (19)$$

$$\Lambda_{\kappa\kappa'} = \frac{1}{N} \sum_{rr'} e^{i(\kappa r - \kappa' r')} \chi_{rr'} \quad (20)$$

For translational invariant systems,  $\Lambda_{\kappa\kappa'}$  is diagonal. In fact, we have  $n_\kappa \equiv \Lambda_{\kappa\kappa} = \Theta[-(\kappa - \kappa_F)] - \Theta[-(\kappa + \kappa_F)]$ , where  $\kappa_F$  is the Fermi momentum. An interesting question is what happens to  $\Lambda_{\kappa\kappa'}$  when we switch on the quasiperiodic perturbation. On the one hand, gaps will open and  $n_\kappa$  will stop being the Heaviside function. On the other, off-diagonal

elements appear in  $\Lambda_{\kappa\kappa'}$  because translational invariance is broken.

We take the Aubry-André model as an example. For the Aubry-André model, different momenta are coupled if  $\kappa - \kappa' = 2\pi\tau j$ ,  $j \in \mathbb{Z}$ , or, for a commensurate approximant with  $\tau_n = F_{n-1}/F_n$ , if  $\kappa - \kappa' = 2\pi\tau_n j$ ,  $j = 0, \dots, N-1$  [11]. Therefore, it is convenient to use  $\kappa_j = 2\pi\tau_c j$  and  $\kappa'_j = 2\pi\tau_c j'$ , with  $j, j' = 0, \dots, N-1$  and define

$$\Lambda_{jj'} = \frac{1}{N} \sum_{rr'} e^{i2\pi\tau_n(jr-j'r')} \chi_{rr'} \quad (21)$$

Note that due to periodic boundary conditions,  $\Lambda_{j+mN, j'+lN} = \Lambda_{jj'}$  for  $m, l \in \mathbb{Z}$ . In order to have an idea on how  $\Lambda_{jj'}$  behaves for  $j \neq j'$ , we define

$$g_\kappa(\epsilon) = \frac{1}{N} \sum_j \Lambda_{j, j+\epsilon} \quad (22)$$

For  $\epsilon = 0$ , we have that  $g(0) = \text{Tr}(|\mathbf{\Lambda}|) = \nu$ , where  $\nu$  is the filling. We define an analogous quantity for the real-space correlation function:

$$g_r(\epsilon) = \frac{1}{N} \sum_r \chi_{r, r+\epsilon} \quad (23)$$

We provide a summary of the results in Fig. 7, for the quarter-filled Aubry-André model. For  $V = 0$ , states with definite crystal momentum  $\kappa$  form the eigenbasis of the Hamiltonian and therefore  $\Lambda_{\kappa\kappa'}$  is a diagonal matrix [which can be seen from the results for  $g_\kappa(\epsilon)$ ], with  $n_\kappa \equiv \Lambda_{\kappa\kappa} = \begin{cases} 1, & |\kappa| \leq \kappa_F \\ 0, & \text{otherwise} \end{cases}$ . From this, one can easily obtain that  $g_r(\epsilon) = \sin(\kappa_F \epsilon)/(\pi \epsilon)$ ,  $\epsilon > 0$ . For  $V > 0$  within the extended phase, we can see that  $\Lambda_{\kappa\kappa'}$  is no longer diagonal, but  $g_\kappa(\epsilon)$  decays exponentially away from the diagonal with

a correlation length  $\xi = 1/\log(2/V)$ , the exactly known correlation length for the extended phase of the Aubry-André model. Furthermore,  $n_\kappa$  develops additional discontinuities at wave vectors  $\kappa_n = \kappa_F + 2\pi\tau n$ ,  $n \in \mathbb{Z}$ , to which the Fermi momentum  $\kappa_F$  couples in perturbation theory [62]. We note however that in practice, the coupling does not occur for any  $n$  due to the finite correlation length  $\xi$ : no gaps open for  $|n| \gg \xi$ . This can give rise to curious situations as the one that we illustrate in Fig. 7 for the quarter-filled Aubry-André model. In this case there is a small-order  $\kappa_n$  corresponding to  $n = -2$  very close to the Fermi momentum  $\kappa_F$  [68], which gives rise to the small momentum windows with large  $n_\kappa$  shown in Fig. 7(a). This translates in the formation of a real-space beating (moiré) pattern with wave vector  $\Delta\kappa = \kappa_F - \kappa_{-2}$ . This can be simply understood if one just considers the diagonal contributions of  $\Lambda_{\kappa\kappa'}$ , given by  $\chi_{rr'} \approx N^{-1} \sum_\kappa e^{-i\kappa(r-r')} n_\kappa$ . Taking the large contributions at  $\kappa \in [\kappa_{-2}, \kappa_F] \cup [-\kappa_F, -\kappa_{-2}]$ , that we call  $\chi_{rr'}^{(\Delta\kappa)}$ , and assuming that they are approximately a constant  $\tilde{n}_{\Delta\kappa}$ , we get  $\chi_{rr'}^{(\Delta\kappa)} \approx (2\pi)^{-1} \tilde{n}_{\Delta\kappa} \left( \int_{-\kappa_F}^{-\kappa_{-2}} + \int_{\kappa_{-2}}^{\kappa_F} \right) d\kappa e^{-i\kappa(r-r')} \sim \cos[\kappa_F(r-r')] + \cos[\kappa_{-2}(r-r')]$ , from which the beating effect seen in  $g_r(\epsilon)$ , in Fig. 7(c), is immediately captured. At the critical point  $V = 2$ , the correlation length diverges and the off-diagonal elements of  $\Lambda_{\kappa\kappa'}$  start to decay in a power-law fashion, as can be seen from the results of  $|g_\kappa(\epsilon)|$ . In this case, the beating effect in  $g_r(\epsilon)$  just mentioned becomes less obvious due to the more complex structure of the momentum-space correlation matrix. Interestingly, using the Aubry-André duality, one can easily check that the real- and momentum-space matrices  $\chi_{rr'}$  and  $\Lambda_{\kappa\kappa'}$  become equal at the critical point. Finally, in the localized phase, the off-diagonal elements of  $\chi_{rr'}$  decay exponentially with the localization length  $\xi = 1/\log(V/2)$ , while the off-diagonal elements of  $\Lambda_{\kappa\kappa'}$  decay with a power-law envelope.

From Fig. 7, we can see that the behaviour of the real- and momentum-space correlation matrices at the critical point is highly non-trivial. In fact, we show in Fig. 8 that there is no clear distinction in the scaling of  $g_r(\epsilon)$  for example critical points that have a significantly different scaling of the entanglement entropy  $\mathcal{C}$ .

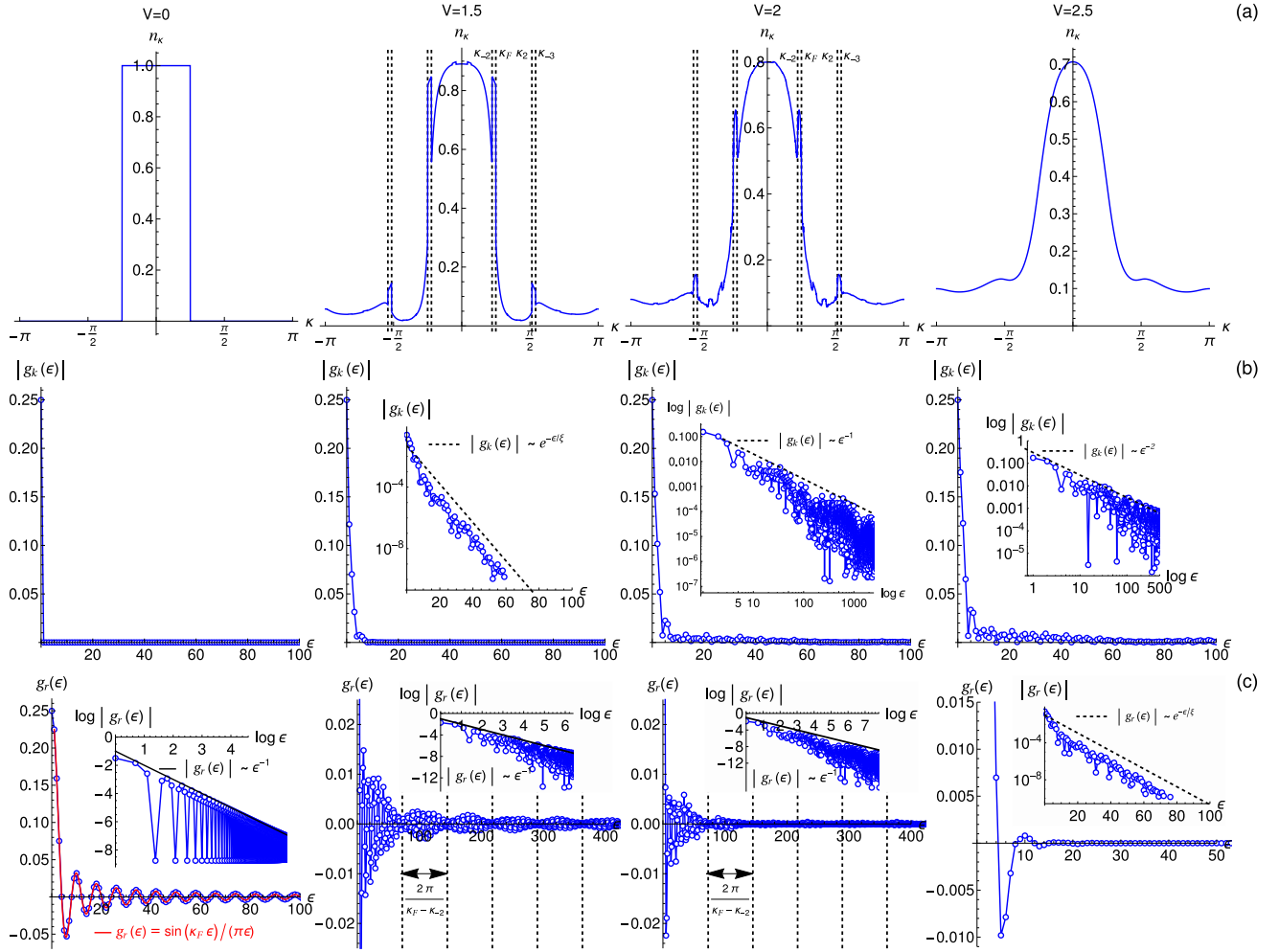


FIG. 7. Results for  $n_\kappa$  (a),  $g_\kappa(\epsilon)$  (b) and  $g_r(\epsilon)$  (c), for the quarter-filled Aubry-André model, for different values of  $V$  in each column (indicated above the corresponding column). In (a) we label some values  $\kappa_n = \kappa_F + 2\pi n$ ,  $n \in \mathbb{Z}$ . (b) The first inset from left to right is a log plot, showing that  $g_\kappa(\epsilon)$  decays exponentially with  $\epsilon$  for  $V = 1.5$ , with a exact correlation length  $\xi = 1/\log(2/V)$ , while the last two insets are log-log plots showing that  $|g_\kappa(\epsilon)|$  decays as a power-law envelope for  $V = 2$  and  $V = 2.5$ . (c) The red line in the leftmost figure corresponds to the exact result  $g_r(\epsilon) = \sin(\kappa_F \epsilon)/(\pi \epsilon)$ , for  $V = 0$ . The first three insets correspond to log-log plots showing the power-law envelop decay of  $|g_r(\epsilon)|$ , while the last plot is a log plot showing the exponential decay for  $V = 2.5$  with the exact localization length  $\xi = 1/\log(V/2)$ . We note that there are moiré patterns that can be noted in the middle figures. These have a periodicity  $\Delta\epsilon = 2\pi/(\kappa_F - \kappa_{-2})$ , where  $\kappa_F$  is the Fermi momentum and  $\kappa_{-2}$  is indicated in (a). All the dashed/full lines in the insets are guides to the eye. The results are all for  $N = 1597$ ,  $\phi = 1.123$ ,  $\kappa = 0.001$ , except for  $V = 2$  where we used  $N = 4181$ . A very small  $\kappa$  was used simply to break fermi-level degeneracies. Note that since this introduces a small imaginary part in  $\chi_{rr'}$ , we just took the real part of  $g_r(\epsilon)$  in the figures.

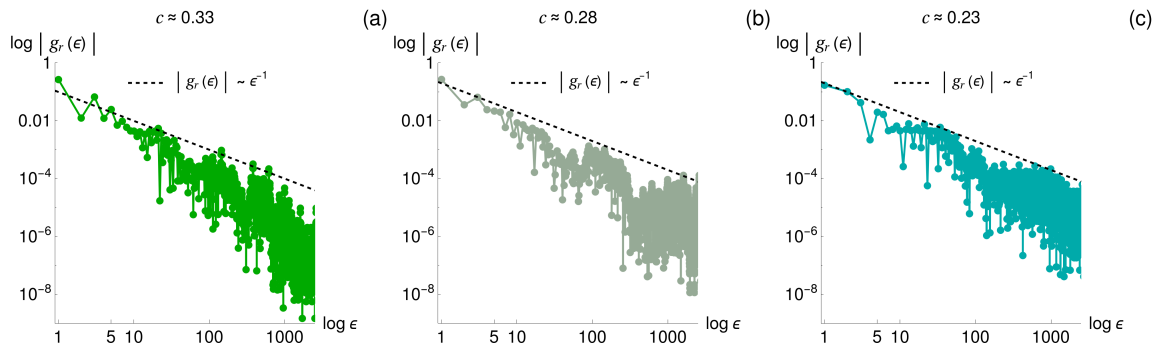


FIG. 8.  $|g_r(\epsilon)|$  at the different critical points also considered in Fig. 2(b). In particular: (a)  $V = 1, \alpha = 2, \rho = 0.47$ ; (b)  $V = 1, \alpha = 2, \rho = 0.538$ ; (c)  $V = 1, \alpha = 0.539, \rho = 0.25$ . The computed entanglement entropy coefficient  $\mathcal{C}$  is indicated above the figure of the corresponding critical point. The dashed black lines are guides to the eye corresponding to a  $|g_r(\epsilon)| \sim \epsilon^{-1}$  scaling.